


# Flattened and broadband mid-infrared supercontinuum generation in $\text{As}_2\text{S}_3$ photonic crystal fibers with a square air-hole lattice

B T Le Tran and L C Van\* 

Department of Physics, Vinh University, 182 Le Duan, Vinh City 461010, Vietnam

Received: 19 October 2023 / Accepted: 04 March 2024

**Abstract:** This paper analyzes smooth and broadband supercontinuum (SC) generation in the mid-infrared range using square-lattice  $\text{As}_2\text{S}_3$ -based photonic crystal fiber (PCF). Simulation of short pulse transmission in optimal PCFs is performed by solving the generalized nonlinear Schrödinger equation with different parameters of pump sources. The first fiber has an anomalous dispersion curve that is flattest and closest to the zero dispersion of all reported fibers. It can generate a broad SC bandwidth covering a 2–11.5  $\mu\text{m}$  range after injecting a pump pulse of 700 pJ energy of (5.83 kW peak power), 120 fs of duration, and 6.5  $\mu\text{m}$  wavelength into 10 cm of fiber length. For the input energy of 810 pJ (9 kW peak power) and pump wavelength of 5  $\mu\text{m}$ , SC spanning 1.9–8.6  $\mu\text{m}$  wavelength region is observed in the second PCF with all-normal dispersion. The achieved SC could find many potential applications in material structure detection, biomedicine, environment monitoring, and food quality control.

**Keywords:** Square photonic crystal fiber; Flattened and broadband supercontinuum generation;  $\text{As}_2\text{S}_3$  chalcogenide glass; Seven air hole rings

## 1. Introduction

Since its first appearance until now, the supercontinuum (SC) has demonstrated its wide range of applications in diverse fields. In optical fibers, essentially, SC generation is a process caused by the interaction of dispersion and many nonlinear effects, i.e. stimulated Raman scattering (SRS), optical wave breaking (OWB), self-phase modulation (SPM), four-wave mixing (FWM), and self-steepening (SS). The importance of mid-infrared (IR) SC generation has been significantly enhanced based on its recent commercial and scientific success. Spectral quality, that is flatness and width, is a necessary condition to increase its application in the fields of biomedicine, food quality control, and environmental monitoring [1–5]. Silica-based fibers with high absorption in the mid-IR range result in SC not being obtained in this zone [6]. Superior to traditional optical fibers, photonic crystal fibers (PCFs) are considered an ideal nonlinear medium that meets essential requirements not only for sensing and multimode support [7, 8] but also for SC generation such as variable dispersion and

high nonlinearity [9–12]. It should be noted that the properties of the pump source used also determine the feasibility of the SC generation process. While spectral flatness is a disadvantage when SC is generated in an anomalous dispersion regime, the opposite trend is achieved in a normal dispersion one. The trade-off is that the bandwidth of the former is much wider than that of the latter. Therefore, with the desire to achieve a coherent and flat SC spectrum, PCFs with flat all-normal dispersion are often preferred which usually ensure uniformity of the pulse (i.e., uniform temporal profile and spectral power density). Whereas, soliton-related effects strongly dominate the spectral broadening in the case of anomalous dispersion [13, 14].

With the ability to expand the spectrum to the mid-IR region, non-silica compounds such as chalcogenide glasses have attracted the attention of the current scientific community. Most glasses in this group possess a broad transmission window and a high nonlinear refractive index [15]. On that basis, several  $\text{As}_2\text{S}_3$ -based PCFs [16] have been designed to enhance the flatness and broadness of mid-IR obtained SCs over 1.85–5.7  $\mu\text{m}$  and 2–10  $\mu\text{m}$  in a 2.5 cm and 5 cm length. Xiao et al. [17] achieved a broadband highly coherent SC of 5973–8695 nm with 6 kW of input power when using  $\text{Ge}_{11.5}\text{As}_{24}\text{Se}_{64.5}$  hexagonal

\*Corresponding author, E-mail: [chuvanlanh@vinhuni.edu.vn](mailto:chuvanlanh@vinhuni.edu.vn)

microstructured fibers. Lanh et al. [18] analyzed the SC spectrum generated in 4000 nm, 3500 nm, and 3000 nm  $\text{As}_{38}\text{Se}_{62}$  PCFs with a hexagonal lattice. The above results are very encouraging, however, the geometric structures of PCFs can be further changed for wide and flat spectra. Many previous studies show that hexagonal-shaped PCFs are good candidates for near-zero flat dispersion configurations but are not SC flatness enhancers [19–21].

We investigate a highly nonlinear  $\text{As}_2\text{S}_3$ -based PCF with a square lattice in this study to obtain flat and broadband SC spectra in short fiber samples. To the best of our knowledge, square PCF is capable of compensating dispersion, enhancing nonlinearity and birefringence, and reducing fiber loss as well [13]. On the other hand, a high nonlinear optical coefficient, low linear and nonlinear loss (two-photon absorption), and a fast response time ( $T < 1$  ps) have made  $\text{As}_2\text{S}_3$  a material of great interest [22]. In this context, As–Se-based materials such as  $\text{As}_2\text{Se}_3$  can become competitive materials due to their high nonlinear refractive index of  $2.4 \times 10^{-17} \text{ m}^2/\text{W}$ , a high refractive index of 2.83 at 1.55  $\mu\text{m}$  and the coefficient low two-photon absorption. Up to now,  $\text{As}_2\text{Se}_3$  has been considered an effective nonlinear medium with high birefringence and nonlinearity to study SC generation in near-IR and mid-IR regions [23]. To further expand the applications of the proposed PCFs, e.g. in all-optical SC switching, non- or less Se composition like  $\text{As}_2\text{S}_3$  becomes more suitable since maintaining a lower value of  $T$ . Another advantage of  $\text{As}_2\text{S}_3$  glass is its high stability against crystallization and flexibility during casting and drawing [24]. Additionally, the core of the proposed PCFs is expanded by controlling the hole pitch and the air-filling factor. This facilitates the coupling process between such fibers and standard ones in practice. The short pulse transmission in the suggested PCFs is then numerically simulated under various parameters.

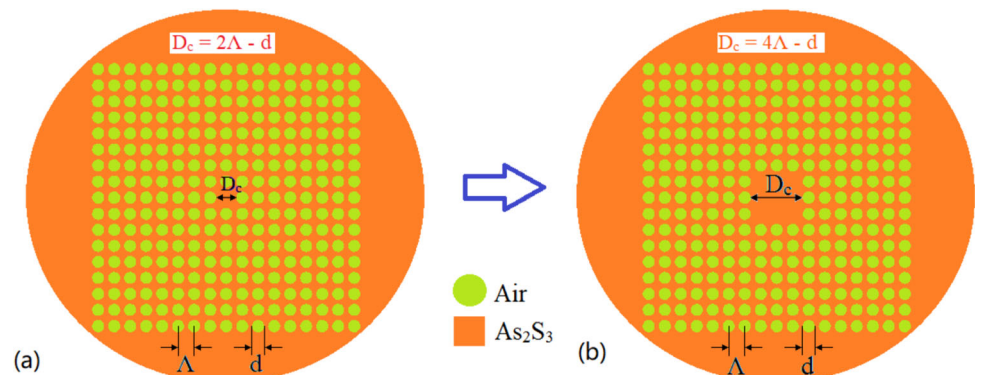
## 2. Theory and modeling

Figure 1(b) depicts the geometrical structure of PCF proposed in our numerical study which can be fabricated using the stack-and-draw technique in the experimental case [25]. The background material is  $\text{As}_2\text{S}_3$  with a wide transmission window in the mid-IR range [26] and a nonlinear refractive index two orders larger than silica at a wavelength of 1.55  $\mu\text{m}$  [27]. The cladding air holes are placed in a square matrix with a hole pitch of  $\Lambda$  and a diameter of  $d$ . The Sellmeier equation [Eq. (1)] is employed to compute the  $\text{As}_2\text{S}_3$  refractive index for which the coefficients are indicated in Table 1 [24]. Recently, a square PCF with an  $\text{As}_2\text{S}_3$  substrate has been investigated with the change of structural parameters [28]. PCF is designed with eight lattice rings to minimize confinement loss, Figure 1(a). However, this comes with the disadvantage of making it difficult to fabricate the optical fiber because the size of the air holes and their spacing need to be controlled precisely. The more rings there are, the more difficult it is to maintain the required precision [25]. Therefore, in this work, a PCF with seven-hole rings is designed after removing the innermost ring. This means that the core dimension is increased by the formulation  $D_c = 4\Lambda - d$ . PCFs with a large core diameter, in fact, can offer SC spectra with high power density in practical applications [18]. One reason for this is that the large core size reduces the confinement loss and increases the effective mode area of the PCF, which enhances the nonlinear effect and broadens the SC spectrum. For example, Hossain et al. [29] reported that a PCF with a core diameter of 1.505  $\mu\text{m}$  achieved an SC spectral bandwidth of 830–2360 nm with 10 pJ of input energy.

$$n = \sqrt{A_0 + \frac{A_1\lambda^2}{\lambda^2 - B_1} + \frac{A_2\lambda^2}{\lambda^2 - B_2} + \frac{A_3\lambda^2}{\lambda^2 - B_3}} \quad (1)$$

The preliminary simulation of the optical properties of the fundamental mode including chromatic dispersion, loss, effective mode area, and effective mode area is worked out using copyrighted software Lumerical Mode

**Fig. 1** Solid-core structure of PCF with square lattice: (a) Ref. [21], (b) in this study



**Table 1** Sellmeier coefficients of As<sub>2</sub>S<sub>3</sub>

Material	A <sub>0</sub>	A <sub>1</sub>	A <sub>2</sub>	A <sub>3</sub>	λ <sub>1</sub> <sup>2</sup>	λ <sub>2</sub> <sup>2</sup>	λ <sub>3</sub> <sup>2</sup>
As <sub>2</sub> S <sub>3</sub>	1	1.8983	1.9222	0.8765	0.2225	0.0625	0.1225

Solutions based on the finite difference eigenmode method [30]. The cross-section of PCF is divided into small rectangular sections called Yee's mesh according to the size of the fiber to increase accuracy in propagation constant calculations. Perfectly matched layer boundary region is assumed as boundary conditions that allow absorbing waves traveling outside the model domain [31].

For SC generation, the chromatic dispersion ( $D$ ) involving the material dispersion ( $D_m$ ) and the waveguide dispersion ( $D_w$ ) is a vital characteristic. The  $D_m$  is determined by Eq. (2), where  $n$  is the refractive index of As<sub>2</sub>S<sub>3</sub> as shown in [24]. Meanwhile, Eq. (3) can be applied to calculate the other [32]:

$$D_m = -\frac{\lambda d^2(n)}{c d\lambda^2} \quad (2)$$

$$D_w = -\frac{\lambda d^2[\text{Re}(n_{\text{eff}})]}{c d\lambda^2} \quad (3)$$

where  $n_{\text{eff}}$  represents the effective refractive index.

The fiber structure and substrate material are factors closely associated with the nonlinearity coefficient, an optical property equally important for SC generation. This can be explained through its definition [33]:

$$\gamma = \frac{2\pi n_2}{\lambda A_{\text{eff}}} \quad (4)$$

where  $n_2$  is the nonlinear refractive index of the material. For the As<sub>2</sub>S<sub>3</sub>-based PCF,  $n_2$  is about  $4.2 \times 10^{-14}$  cm<sup>2</sup>/W at 1.3 μm and remains almost unchanged over a wide range of wavelengths [24]. The greater the nonlinear refractive index, the higher the nonlinearity. As a result, to further improve the nonlinearity of PCF, materials possessing high  $n_2$  are required. Moreover,  $A_{\text{eff}}$ , means the effective mode region can be easily adjusted through the fiber parameters. By the use of the full-vectorial finite element method, the chromatic dispersion and nonlinear features in PCFs are accurately simulated.

It is possible to investigate SC generation in PCF through the calculation of Eq. (5), the so-called generalized nonlinear Schrödinger equation (GNLSE) [34]:

$$\begin{aligned} \frac{\partial A}{\partial z} + \frac{1}{2}\alpha A - \sum_{n \geq 2} \beta_n \frac{i^{n+1} \partial^n A}{n! \partial t^n} = i\gamma a \\ + i\gamma \frac{i\partial}{\omega_0 \partial t} \left( A(z, T) \int_{-\infty}^{+\infty} R(t') |A(z, t-t')|^2 dt' \right) \end{aligned} \quad (5)$$

In Eq. (5), the coefficients  $\alpha$  and  $\beta_n$  are the total attenuation and the  $n$ -th derivative of the propagation constant  $\beta$ , correspondingly. In fact, the evolution of the short pulse is ruled by  $\beta_n$  regarding the extension of the Taylor series of the propagation constant  $\beta$ . The pulse envelope  $A$  with a fiber length of  $z$  and a time variable of  $t$ . The input pulse selected here is the unchirped hyperbolic secant pulse, where  $t_0$  represents the duration and is determined by the ratio between full width at half maximum (FWHM) and 1.7627.  $P_0$  is the peak power [35].

$$A(0, t) = \sqrt{P_0} \text{sech}\left(\frac{t}{t_0}\right) \quad (6)$$

An equally important parameter on the right side of Eq. (5) is  $R(t')$ . This is the combined function of the nonlinear and Raman response given by [36]:

$$R(t') = \delta(t')(1 - f_R) + f_R \frac{\tau_1^2 + \tau_2^2}{\tau_1 \tau_2} \exp\left(\frac{-t'}{\tau_2}\right) \sin\left(\frac{-t'}{\tau_1}\right) \quad (7)$$

In Eq. (7), the Raman response contribution is described by  $f_R$ ;  $\tau_1$  and  $\tau_2$  are two adjustable parameters. According to the publication [24], the values of the above three factors are 0.2 of  $f_R$ , 15.5 fs of  $\tau_1$ , and 230.5 fs of  $\tau_2$  as for As<sub>2</sub>S<sub>3</sub>. These numbers demonstrated a well-suited between the modeling and the actual Raman spectra in As<sub>2</sub>S<sub>3</sub> PCFs.

The split-step Fourier method (SSFM) is by far the most widely used to solve GNLSE [34]. In the case of SSFM, the linear and nonlinear terms acting simultaneously during pulse propagation along the fiber are independently integrated. The results are then combined to gain the final solution. Suppose that the total path of the pulse propagation in the fiber is divided into very short sections with a length of  $h$ . The simplest split-step scheme consists of first dividing the initial pulse with Fourier transform  $A(z, \omega)$  into short segments of length  $h$  affected by dispersion, followed by the same step size only influenced by nonlinear effects (or vice-versa):

$$\begin{aligned} A(z+h, t) = \left[ \exp\left(\frac{h}{2} \hat{L}\right) \right] \left[ \int_z^{z+h} \exp(h\hat{N}) A_N(z, t) dz \right] \\ \times \left[ \exp\left(\frac{h}{2} \hat{L}\right) \right] A(z, t) \end{aligned} \quad (8)$$

where  $A(z + h, t)$  is a result of the process of half a linear step, a full nonlinear step, and then the last half linear step. A fourth-order Runge–Kutta method is employed for  $NA_N$  numerical integration, which requires four evaluations of  $N$  [37]. The Fourier transform operation is worked out using a fast Fourier transform (FFT) algorithm [38]. It is possible to reach  $A$  in the time domain with two FFTs for step  $h$ , i.e. one FFT and one inverse FFT, in the case of neglecting self-steepening and the delayed Raman response. This can result in approximately 6.5 times faster computation compared to the scheme involving fourth-order Runge–Kutta numerical integration.

### 3. Results and discussions

#### 3.1. SC generation in anomalous dispersion regime

Optimization of the structural parameters of the  $As_2S_3$ -based PCFs such as hole pitch  $\Lambda$  and air-filling ratio  $d/\Lambda$  is necessary to achieve near-zero flattened dispersion in a wide wavelength range. The impact on the dispersion of  $\Lambda$  and  $d/\Lambda$  is illustrated in Figures 2(a) and 2(b). The hole pitch is changed from 2 to 3 corresponding with 0.3–0.7 of the filling ratio change. The results from Figure 2 show that the dispersion curve is assigned in both normal and anomalous dispersion ranges in the small core PCFs ( $\Lambda = 2 \mu\text{m}$ ). Here, we obtain a fiber structure ( $d/\Lambda = 0.3$ ) whose dispersion curve lies entirely in the normal dispersion region with  $D < -10 \text{ ps/nm/km}$  in the 3.5–6.5  $\mu\text{m}$  wavelength range. This curve tends to move above the zero dispersion line to possess two ZDWs when  $\Lambda$  increases to 3  $\mu\text{m}$ . Meanwhile, the anomalous dispersion regime is still maintained for the remaining structures despite the change in hole pitch. On the other hand, increasing  $d/\Lambda$  leads to an

improvement in the flatness of the  $D$  curves in the wavelength range larger than 4  $\mu\text{m}$ . This means that the fiber with  $d/\Lambda = 0.7$  has the flattest dispersion profile even though it is farthest away from the zero dispersion in this area. It can be predicted that while the dispersion profile depends on  $\Lambda$ , the dispersion smoothness and flat dispersion range are mainly determined by  $d/\Lambda$ . That is the reason why PCFs with optimal dispersion can be obtained by controlling these two parameters.

Our goal is to design SC sources with a broad and smooth spectrum, and thus fiber structures with near-zero flat dispersion curves and ZDW compatible with the pump wavelength are required [36]. As mentioned earlier, fibers with anomalous dispersion often have superior spectral broadening with the help of soliton dynamics. Meanwhile, a smooth and coherent SC bandwidth is expected when pumping in the normal dispersion region of PCF. Therefore, the optimal parameter sets that satisfy the above criteria are chosen after a series of simulations. The first fiber with anomalous dispersion  $F_1$ :  $\Lambda = 3 \mu\text{m}$ ,  $d/\Lambda = 0.3$ ,  $D_c = 11.1 \mu\text{m}$  expected to be pumped at 6.5  $\mu\text{m}$ . Two ZDWs of  $F_1$  are 4.54  $\mu\text{m}$  and 8.87  $\mu\text{m}$ , respectively. With the optimized geometrical parameters, chromatic dispersion  $D$ , confinement loss  $\alpha_c$ , nonlinear coefficient  $\gamma$ , and effective mode area  $A_{\text{eff}}$  of  $F_1$  at pump wavelengths are depicted in Figure 3(a). The value of the nonlinear coefficient is greater than  $50 \text{ W}^{-1} \text{ km}^{-1}$  in the flat dispersion range generating a wide SC generation. Experimental results show that the material loss of  $As_2S_3$  is 0.4 dB/m in the 1–2.5  $\mu\text{m}$  wavelength range [39]. When the wavelength is greater than 2.25  $\mu\text{m}$ , confinement loss tends to exceed this value resulting in it being considered a propagation loss. In addition, the high transparency and high  $n_2$  of  $As_2S_3$  [24, 40] allow the generation of SC in an optical fiber of a few centimeters long without considering

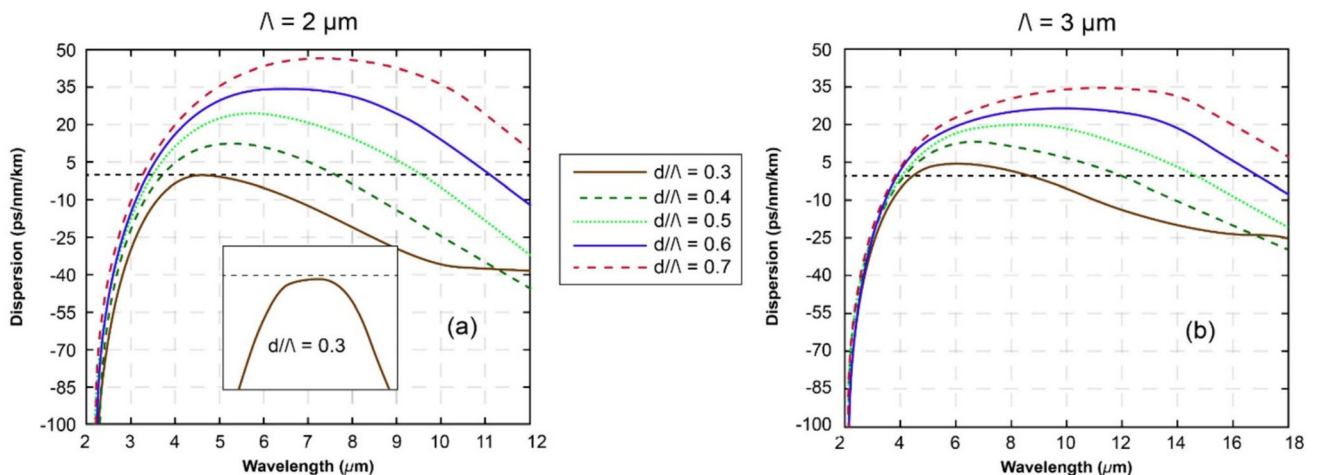
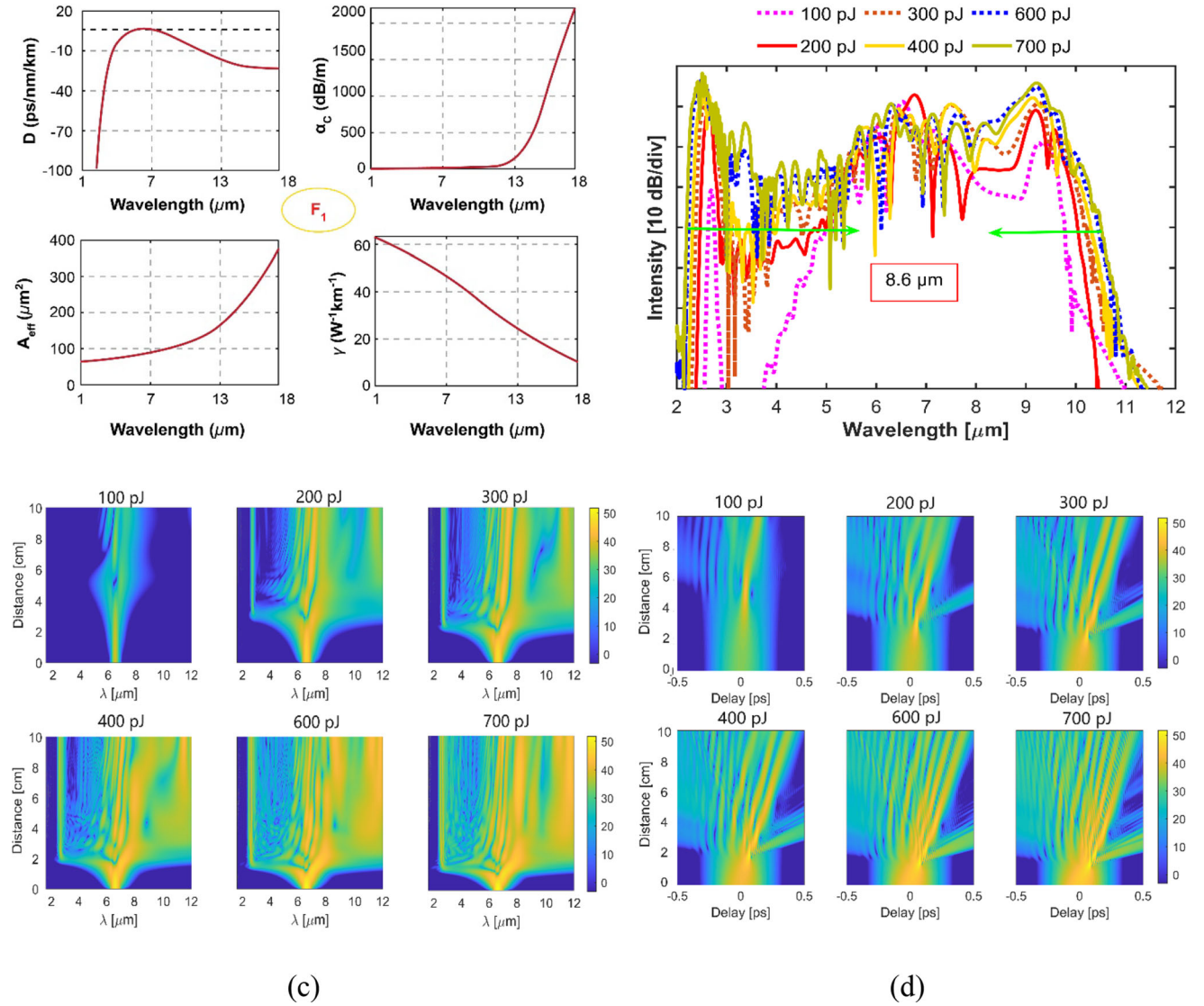


Fig. 2 Dispersion characteristics of the  $As_2S_3$ -based PCFs for  $d/\Lambda = 0.3$ –0.7 and the hole pitch of 2 and 3  $\mu\text{m}$



**Fig. 3** For  $F_1$ : (a) Linear and nonlinear characteristics. (b) The output spectrum of the SC for various input energy. (c) The SC evolution along the fiber length and (d) the corresponding time domain representation of the pulse propagation with various input energy levels

material loss. The confinement loss coefficient of  $F_1$  fiber is  $4.5 \times 10^{-4}$  dB/m at 6.5 μm, much smaller than the 0.0117 dB/m of fiber in [41] pumped at 3.25 μm. Alternatively,  $\sim 27$  dB/m confinement loss at 7 μm was achieved Ge<sub>10</sub>As<sub>22</sub>Se<sub>68</sub>-based PCF [42], which is higher than that of  $F_1$  fiber.

Figure 3(b) shows the output spectrum of  $F_1$  fiber with the following pump pulse parameters: energy of 100–700 pJ, fiber length of 10 cm, and pulse width of 120 fs. The noise profile of the SC in the anomalous regime of dispersion is indisputable because soliton dynamics can be extremely sensitive to the slightest fluctuations (including quantum noise) in the input pulses [43]. The SC spectrum covering the wavelength range 2–11.5 μm with a FWHM of 8.6 μm achieved at the greatest energy of 700 pJ. Figure 3(c) and Figure 3(d) show the evolution of the SC

spectrum in the anomalous dispersion regime along the length of  $F_1$  fiber and the corresponding time domain representation of the pulse propagation with various input energy levels. The impact of nonlinear effects and dispersion on the pulses depends on the difference in the fiber length compared to the dispersion length ( $L_D$ ) as well as the nonlinear length ( $L_{\text{NL}}$ ) [44]. Nonlinear effects control the degree of spectral broadening at the initial time of pulse propagation along the fiber. There is a surge in the dominant role of dispersion in further propagation. Indeed, at the second-order dispersion coefficient  $\beta_2 = -0.11885$  ps<sup>2</sup> m<sup>-1</sup>,  $L_{\text{NL}} = 1/\gamma P_0 = 0.38$  cm is shown to be much smaller than  $L_D = t_0^2/\beta_2 = 12$  cm. In fact, solitons cannot exist if too low input pulse energies are used. This explains the symmetric profile and narrow bandwidth of the

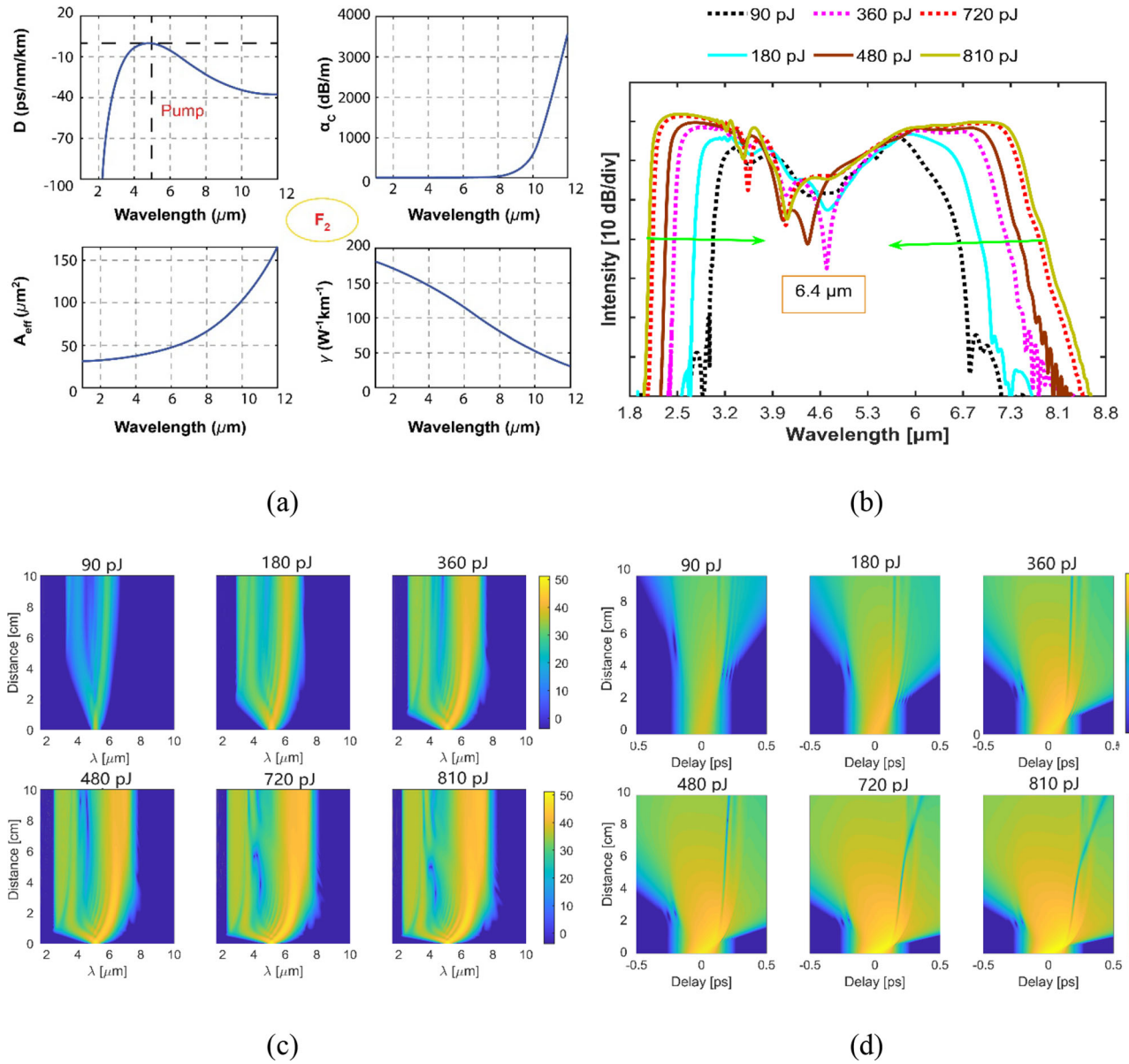


**Fig. 4** For  $F_2$ : (a) Linear and nonlinear characteristics. (b) The output spectrum of the SC for various input energy. (c) The SC evolution along the fiber length and (d) the corresponding time domain representation of the pulse propagation with various input energy levels

spectrum at 100 pJ, where the influence of SPM is favored. However, this state does not last long as input energy increases. Soliton fission begins at an input pulse energy of 200 pJ. Dispersive wave dynamics are responsible for generating new wavelength bands in the normal dispersion regime. However, the steep slope of dispersion in this region and the large effective mode area on the red wavelength side halt the increasing trend of the SC bandwidth at a large enough energy such as 600 pJ. The spectrum due to SPM is also affected by dispersion during further propagation, and the short wavelengths at the trailing edge travel slower than spectral components of the input pulse tail. The overlap between the pulse tail and

trailing edge suddenly generates new wavelengths by the degenerated FWM process, which are attributed to OWB [45]. Once the solitons move further, the impact of the Raman soliton self-frequency shift [46] is taken into account leading to their shift towards longer wavelengths. FWM gives rise to a dispersive wave effect that propagates ignoring the frequency shift. After a propagation length of 2 cm, the spectral bandwidth remains fairly constant because of the steep integrated dispersion curve on both sides. Additionally, the larger time delay between different frequencies is observed in a longer propagation.

**Table 2** Comparison of SC bandwidth in our work with previous publications

Chalcogenide glass	References	$P_0$ (kW)	Pump wavelength ( $\mu\text{m}$ )	SC spectral range ( $\mu\text{m}$ )	Spectral width ( $\mu\text{m}$ )	Regime
As <sub>2</sub> S <sub>3</sub> , F <sub>1</sub>	This work	5.83	6.5	2–11.5	8.6	Anomalous
As <sub>2</sub> Se <sub>3</sub>	[36]	7.5	3.5	2–10	8	Anomalous
As <sub>39</sub> Se <sub>61</sub>	[51]	15	2.45	1.4–4.2	2.8	Anomalous
As <sub>2</sub> S <sub>3</sub>	[52]	380	4.2	1.7–4.8	3.1	Anomalous
As <sub>2</sub> Se <sub>3</sub>	[53]	2890	9.8	2–5.1	3.1	Anomalous
Ge <sub>15</sub> Ga <sub>3</sub> Sb <sub>12</sub> S <sub>70</sub>	[54]	40,000	2.3	0.95–3.35	2.4	Anomalous
As <sub>2</sub> S <sub>3</sub>	[48]	200	3	1.6–4.8	3.2	Anomalous
As <sub>2</sub> S <sub>3</sub> , F <sub>2</sub>	This work	9	5	1.9–8.6	6.4	All-normal
As <sub>2</sub> S <sub>5</sub>	[55]	10.12	2.6	1.6–3.7	2.1	All-normal
Ge–As–Se	[56]	16.5	4	3–6	3	All-normal

### 3.2. SC generation in normal dispersion regime

The influence of pump parameters on an all-normal dispersion SC generation in F<sub>2</sub> is investigated in Figure 4. The design parameters of this PCF, in turn, are as follows:  $A = 2 \mu\text{m}$ ,  $d/A = 0.3$ ,  $D_c = 7.4 \mu\text{m}$ . In this case, the broadest SC spectrum can be obtained by using a pump wavelength near the one at the local maximum point of the dispersion curve. With the geometrical parameters are optimized, the highest value of the dispersion curve is around  $-0.08 \text{ ps/nm/km}$  at the wavelength of  $4.82 \mu\text{m}$ . The measurements of bulk material loss of As<sub>2</sub>S<sub>3</sub> chalcogenide in publication [47] show the peaks in the material loss curve of As<sub>2</sub>S<sub>3</sub> at wavelengths of  $2.8 \mu\text{m}$ ,  $2.92 \mu\text{m}$ , and  $4.05 \mu\text{m}$  because of the absorption bands of impurities of H<sub>2</sub>O, OH, and SH, respectively. Furthermore, Si et al. [48] reported that a strong absorption measured by the cut-off method using a Fourier transform infrared spectrophotometer peak occurs at  $4.5 \mu\text{m}$  in As<sub>2</sub>S<sub>3</sub> PCFs. In contrast, the loss at  $5 \mu\text{m}$  is quite low, equivalent to where the loss reaches its lowest value,  $3.8 \mu\text{m}$ . For those reasons, F<sub>2</sub> fiber is pumped by a femtosecond laser with a pump duration of 90 fs and a pump wavelength of  $5 \mu\text{m}$  to limit as much attenuation as possible which could negatively affect the spectrum broadening. The  $D$ ,  $A_{\text{eff}}$ ,  $\gamma$ , and  $\alpha_c$  configurations are similar to the F<sub>1</sub> fiber. Their values are  $-0.5 \text{ ps/nm/km}$ ,  $39.74 \mu\text{m}^2$ ,  $132.74 \text{ W}^{-1} \text{ km}^{-1}$ ,  $5.95 \times 10^{-3} \text{ dB/m}$ .

The SC generation in all-normal dispersion fiber is analyzed with 90 fs duration and different input pulse energies. The F<sub>2</sub> length is assumed to be 10 cm, the same as F<sub>1</sub>. Figure 4(b)–4(d) clearly show that F<sub>2</sub> fiber requires higher energy of input laser pulses than SC generation pumped into anomalous dispersion wavelengths of F<sub>1</sub>. The spectral bandwidth of F<sub>2</sub> is also narrower than that of F<sub>1</sub>. The smooth and flat SC profile, however, is the first good

impression noticed in SC generation in an all-normal dispersion regime. If soliton dynamics disrupt the integrity of the pump pulse in F<sub>1</sub>, this is eliminated in fiber F<sub>2</sub>. SPM is considered to be dominant in the spectral broadening mechanism after the side lobe of the spectrum is formed. Next, OWB gradually appears at the trailing edge due to the impact of SS causing a loss of symmetry on the blue-shift wavelength side of SC [49]. As a result, new wavelengths are not created despite further propagation because it requires the pulse tail to overlap with the SPM-induced components. On the other side, OWB also exerts its influence with a narrow spectral range because of limited phase-matching conditions as well as reduced nonlinearity [50]. After completing 10 cm of propagation, the all-normal dispersion SC generation in the F<sub>2</sub> fiber has a spectral bandwidth of  $1.9\text{--}8.6 \mu\text{m}$  within 10 dB. On the other hand, the time delay between different frequencies having different velocities tends to be larger when increasing the propagation distance.

Comparison between SC generation properties using chalcogenide PCFs demonstrates outstanding pros of the proposed PCFs in terms of spectral width and cost reduction. Detailed data are shown in Table 2. For instance, PCFs with Ge–As–Se glasses require up to 16.5 kW to expand the spectrum from 3 to  $6 \mu\text{m}$  [56]. Meanwhile, F<sub>2</sub> fiber can drop the power by nearly half, that is, 9 kW to obtain the SC range of  $1.9\text{--}8.6 \mu\text{m}$ . Recently, the publication [36] also achieves spectral width equivalent to F<sub>1</sub> fiber but must use a larger peak power. Even in this regime, a Ge<sub>15</sub>Ga<sub>3</sub>Sb<sub>12</sub>S<sub>70</sub> PCF with a spectral range of  $0.95\text{--}3.35 \mu\text{m}$  with a power of up to 40,000 kW is observed [54]. We consider here peak power instead of pump energy to demonstrate the potential of the proposed fibers in all-fiber SC systems.

## 4. Conclusion

Introducing a large core region in an  $\text{As}_2\text{S}_3$ -based PCF with a square lattice and selecting appropriate sets of parameters can achieve near-zero flattened dispersion profiles in the mid-IR range. Numerical simulations of the SC generation in the proposed PCF are then performed considering how the flatness and bandwidth of the spectrum are affected by the pumping parameters. As a result, a smooth SC with a bandwidth of 2–11.5  $\mu\text{m}$  using a femtosecond laser with 6.5  $\mu\text{m}$  wavelength, 120 duration to inject into 10 cm-length  $F_1$ . Such SC is suitable for low-noise amplifiers in the mid-IR range such as Praseodymium doped fiber amplifiers [57]. Meanwhile, two-octave SC generation, that is 1.9–8.6  $\mu\text{m}$ , is generated in  $F_2$  fiber when the pump wavelength used is 5  $\mu\text{m}$ . To the best of our knowledge, this is a much wider SC than previous publications [36, 48, 51–54] which have a high potential for selective and rapid detection of nerve agent simulants [58]. Additionally, the advantage of the large core diameter also increases the coupling efficiency between these fibers and standard fibers if considering compact all-fiber SC generation systems [36].

**Acknowledgements** Not applicable.

**Author contributions** All authors contributed to the study's conception and design. LCV: Conceptualization, Methodology, Writing—original draft, Supervision, Writing—review & editing. BTLT: Writing—original draft, Visualization, Investigation, Data curation.

**Data availability** Not applicable.

**Code availability** Not applicable.

**Declarations**

**Conflict of interest** The authors have no relevant financial or non-financial interests to disclose.

## References

- [1] C S Brès, A D Torre, D Grassani and V Brasch *C Grillet and C Monat Nanophotonics* **12** 1199 (2023)
- [2] G P Agrawal *Nonlinear fiber optics* (Berlin, Heidelberg, Springer, 2000)
- [3] A Ghanbari and A Kashaninia *A Sadr and H Saghaei Optik* **140** 545 (2017)
- [4] J Swiderski *Prog. Quant. Electron.* **38** 189 (2014)
- [5] K Xia, L Yang, B Yan, J Liu, X Li, R Zhao and P Yang *Laser Tech.* **127** 106204 (2020)
- [6] T Wang, F Pang, S Huang and J Wen *Infor. Tech. Electron. Engineering* **20** 481 (2019)
- [7] B Kuri, B Dutta, N Sarkar, S Santra, P Mandal, K Mallick and A S Patra *Result in Phys.* **36** 105465 (2022)
- [8] M J B M Leon and A S Disha *Sens. Inter.* **2** 100115 (2021)
- [9] H T Duc, L T B Tran and V D Long *Development J.* **25** 2581 (2022)
- [10] H Yang and J Ni *Optik* **125** 4367 (2014)
- [11] X Alishacelestin, A S Raja and S Selvendran *Laser Phys.* **31** 065101 (2021)
- [12] Y Ma, R Wan, S Li, L Yang and P Wang *Materials (Basel)* **15** 1558 (2022)
- [13] C V Lanh and L T B Tran *Laser Phys.* **33** 095102 (2023)
- [14] M R Karim et al *IEEE Photon. Tech. Lett.* **29** 1972 (2017)
- [15] C V Lanh, L T B Tran, D V Trong, V T M Ngoc, N T Thuy and N T H Phuong *Fiber Tech.* **75** 103151 (2023)
- [16] W Yuan *Laser Phys. Lett.* **10** 095107 (2013)
- [17] K Xiao, Y Ye and R Min *Front. Phys.* **10** 933010 (2022)
- [18] C V Lanh, D X Khoa, L C Trung, T D Thanh and N T Thuy *Materials* **137** 113547 (2023)
- [19] S Sen, Md Abdullah-Al-Shafi and M A Kabir *Sens. Bio-Sens. Research* **30** 100377 (2020)
- [20] H T Duc, N A Tu and N T Thuy *VNU J. Science Mathematics—Phys.* **39** 42 (2023)
- [21] G K M Hasanuzzaman, T M Sakib and A K Paul *Sens. Bio-Sens. Research* **42** 100582 (2023)
- [22] A Patel, D Singh, Y Sonvane, P B Thakor and R Ahuja *Computational Materials Science* **183** 109913 (2020)
- [23] N T Thuy, H T Duc and C V Lanh *Opt. Quant. Electron.* **56** 367 (2024)
- [24] A K M S J Choyon and R Chowdhury *Optik* **258** 168857 (2022)
- [25] L R Murphy, S Yerolatsitis, T A Birks and J M Stone *Optics Express* **30** 37303 (2022)
- [26] X Zhang, M He, M Chang, H Chen, N Chen, N Qi, M Yuan and X Qin *Opt. Communications* **410** 396 (2018)
- [27] M Asobe, T Kanamori, K Naganuma, H Itoh and T Kaino *J. Appl. Phys.* **77** 5518 (1995)
- [28] D V Trong, L T B Tran, H T A Thu, N T Thuy and C V Lanh *Vinh Uni. J Science* **51** 44 (2022)
- [29] M B Hossain, A A M Bulbul, M A Mukit and E Podde *Opt. Photon. J.* **7** 235 (2017)
- [30] <https://www.lumerical.com/products/mode/>
- [31] Y B Yang, J Li, Q Q Nie, Z Y Zhou and H Xu *Eng. Analysis with Boundary Elements* **155** 528 (2023)
- [32] I Ayesta, J Zubia, J Arrue, M A Illarramendi and M Azkune *Polymers* **9** 730 (2017)
- [33] X Liu, Z Yang, D Wang and H Cao *Crystals* **6** 158 (2016)
- [34] S M Salimullah and M Faisa *Alexandria Engineering J.* **70** 289 (2023)
- [35] A F Abas, K Y Lau, Y M Al-Moliki, Y T Aladadi, M T Alreashedi and M A Mahdi *Appl. Sci.* **13** 4087 (2023)
- [36] C V Lanh, N T Thuy, L T B Tran, H T Duc, V T M Ngoc, L V Hieu and H V Thuy *Photonics and Nanostructures—Fundamentals and Appl.* **48** 100986 (2022)
- [37] M M Shior, B C Agbata, G O Acheneje, G D Gbor and S Musa *East African Scholars J. Eng. Comput. Sci.* **6** 1 (2023)
- [38] A Medjouria and D Abed *Opt. Mat.* **9** 109391 (2019)
- [39] W Geng, C Bao, Y Fang, Y Wang, Y Li, Z Wang, Y G Liu, H Huang, Y Ren, Z Pan and Y Yue *IEEE Access* **8** 168177 (2020)
- [40] G E Snopatin, I V Skripachev, V G Plotnichenko and M F Churbanov *Dokl. Chem.* **511** 187 (2023)
- [41] L T B Tran, N M Thien, N T Nam, D T Tuyet, T D Tan, M V Luu, N T Vinh and C V Lanh *In Proc. the 8<sup>th</sup> Academic Conf. Natural Sci. Young Scientists, Master and PhD. Students from Asean Countries (CASEAN-8)*, 463 (2023)
- [42] C R Petersen, R D Engelsholm, C Markos, L Brilland, C Cailaud, J Trolès and O Bang *Opt. Express* **25** 15336 (2017)
- [43] A Efimov and A J Taylor *Opt. Express* **16** 5942 (2008)
- [44] Y Gao, X Wang, X Zhu, K Zhao, H Liu, Z Wang, S Fang and Z Wei *Phys. Rev. Research* **4** 013035 (2022)
- [45] D V Trong and C V Lanh *Phys. Lett. B* **37** 2350063 (2023)



- [46] M Karpov, H Guo, A Kordts, V Brasch, M H P Pfeiffer, M Zervas, M Geiselmann and T J Kippenberg *Phys. Rev. Lett.* **116** 103902 (2016)
- [47] C Wei, J Hu and C R Menyuk *Frontiers in Phys.* **4** 30 (2016)
- [48] N Si, L Sun, Z Zhao, X Wang, Q Zhu, P Zhang, S Liu, Z Pan, Z Liu, S Dai and Q Nie *Appl. Phys. A* **124** 171 (2018)
- [49] V Dagytė and N Anttu *Nanotechnology* **30** 025710 (2019)
- [50] C Manzoni and G Cerullo *J. Opt.* **18** 103501 (2016)
- [51] S O Leonov, Y Wang, V S Shiryaev, G E Snopatin, B S Stepanov, V G Plotnichenko, E Vicentini, A Gambetta, N Coluccelli, C Svelto, P Laporta and G Galzerano *Opt. Lett.* **45** 1346 (2020)
- [52] Z Eslami, P Ryczkowski, L Salmela and G Genty *Opt. Lett.* **45** 3103 (2020)
- [53] T Cheng, K Nagasaka, T H Tuan, X Xue, M Matsumoto, H Tezuka, T Suzuki and Y Ohishi *Opt. Lett.* **41** 2117 (2016)
- [54] T Cheng, H Kawashima, X Xue, D Deng, M Matsumoto, T Misumi, T Suzuki and Y Ohishi *J. Light. Technol.* **33** 333 (2015)
- [55] T S Saini, T H Tuan, T Suzuki and Y Ohishi *Sci. Rep.* **10** 2236 (2020)
- [56] M Meneghetti, X Forestier, C R Petersen, R Kasztelanic, M Klimczak, O Bang, R Buczyński and J Troles *Adv. Photonics Res.* **2** 2000091 (2021)
- [57] A G Alharbi, J Mirza, M Raza and S Ghafoor *Computers Mat. Continua* **73** 5411 (2022)
- [58] F W Dagnaw, W Feng and Q H Song *Sens. Actuators B: Chemical* **318** 127937 (2020)

**Publisher's Note** Springer Nature remains neutral with regard to jurisdictional claims in published maps and institutional affiliations.

Springer Nature or its licensor (e.g. a society or other partner) holds exclusive rights to this article under a publishing agreement with the author(s) or other rightsholder(s); author self-archiving of the accepted manuscript version of this article is solely governed by the terms of such publishing agreement and applicable law.